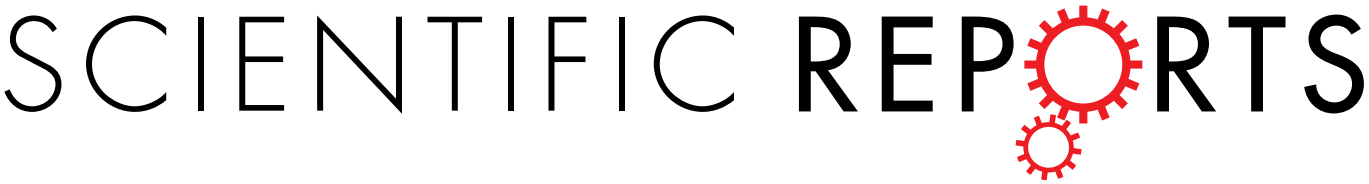

OPEN

Electron spin relaxations of phosphorus donors in bulk silicon under large electric field

Received: 19 September 2018
Accepted: 21 January 2019
Published online: 27 February 2019

Daniel K. Park[1,2], Sejun Park[1], Hyejung Jee[1,3] & Soonchil Lee[1]

Modulation of donor electron wavefunction via electric fields is vital to quantum computing architectures based on donor spins in silicon. For practical and scalable applications, the donor-based qubits must retain sufficiently long coherence times in any realistic experimental conditions. Here, we present pulsed electron spin resonance studies on the longitudinal (T_1) and transverse (T_2) relaxation times of phosphorus donors in bulk silicon with various electric field strengths up to near avalanche breakdown in high magnetic fields of about 1.2 T and low temperatures of about 8 K. We find that the T_1 relaxation time is significantly reduced under large electric fields due to electric current, and T_2 is affected as the T_1 process can dominate decoherence. Furthermore, we show that the magnetoresistance effect in silicon can be exploited as a means to combat the reduction in the coherence times. While qubit coherence times must be much longer than quantum gate times, electrically accelerated T_1 can be found useful when qubit state initialization relies on thermal equilibration.

Phosphorus donor spins in silicon (Si:P) are promising candidates for encoding quantum information due to outstanding coherence times and the availability of the mature semiconductor industry. Since the quantum computing architecture based on donor spins in silicon was proposed by Kane[1], many significant milestones, such as extending qubit coherence times via silicon-28 isotope enrichment[2–6], high-fidelity control and readout of single donor spins[7–10], and resonance frequency tuning using electric fields induced Stark shift for the qubit-selective control[11,12], have been achieved. Also, several device designs within the donor-based framework have been proposed[13–15] to enable topological quantum error correction. However, realizing two-qubit quantum operations using the exchange interactions as originally proposed by Kane in a scalable manner remains challenging due to the extreme sensitivity of the interaction strength to the donor displacement. To relax the requirement on the spatial precision, an architecture that exploits electric dipole interactions was recently proposed[16]. In this approach, the qubit is defined using the flip-flop energy splitting of the nuclear and electron spin states, and is called the flip-flop qubit. One and two qubit gate implementations require shifting the donor electron wavefunction to the ionization point, where the electron is shared halfway between donor and Si/SiO_2 interface, via electric fields. This scheme allows for the larger inter-qubit spacing than the exchange-based method, which yields sufficient room to place classical control and readout components[16]. After all, the application of electric fields is ubiquitous in various proposals for donor-based quantum information processing. On the other hand, theoretical analyses of the single-donor flip-flop qubit with reasonable experimental parameters predicted considerable decrease of the qubit T_1 relaxation time due to strong interaction with phonon-induced deformation potentials and the nontrivial valley-related characteristics of the electron-phonon interaction and the involved electronic states[17]. Yet, the effect of electric fields near ionization on the T_1 and T_2 times of donor spins in silicon with higher qubit densities is not clear-cut.

This work reports a detailed experimental study on the spin relaxation times of phosphorus (^{31}P) donor electrons in bulk silicon under electric fields (E_0) ranging up to near avalanche breakdown triggered by impact ionization using pulsed electron spin resonance (ESR). Two Si:P wafers with donor concentrations of about 10^{14}–10^{15} P/cm^3 are tested in the external static magnetic field (B_0) strength of about 1.2 T and at temperatures near 8 K for

[1]Department of Physics, Korea Advanced Institute of Science and Technology, Daejeon, 34141, Korea. [2]Present address: School of Electrical Engineering, Korea Advanced Institute of Science and Technology, Daejeon, 34141, Korea. [3]Present address: Department of Physics, Imperial College London, London, SW7 2BW, United Kingdom. Correspondence and requests for materials should be addressed to D.K.P. (email: kpark10@kaist.ac.kr) or S.L. (email: soonchillee@kaist.ac.kr)

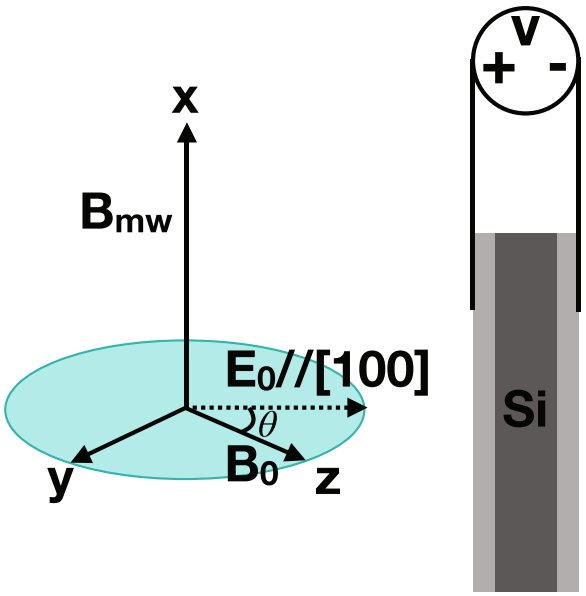

Figure 1. Schematic of the Si:P wafer (dark gray) with aluminum (light gray) sputtered on two faces of the wafer (not in scale) and its orientation with respect to external fields. The electric field, E_0, is formed between the metal plates by applying DC voltage. The sample is inserted in the static magnetic field, B_0, in such a position that the direction of the electric field is coplanar to the magnetic field. The microwave field, B_{mw}, for controlling electron spins points perpendicular to both E_0 and B_0. The coordinate frame on the left is arbitrarily defined for convenience.

good compromise between the detection sensitivity and the T_1 relaxation time in the absence of electric field. The key findings are summarized as follows. The T_1 relaxation time changes dramatically under strong electric field near (but before) the avalanche breakdown, and the coherence time T_2 is limited by T_1. This is attributed to the electric current (I) in the bulk silicon. However, due to magnetoresistance in silicon[18,19], the amount of electric current varies with the orientation of the electric field with respect to the magnetic field. Therefore, the reduction in the relaxation times can be minimized by carefully determining the orientation.

Results

The spin relaxation times of the donor-bound electrons are measured from two Si:P wafers, A and B, with phosphorus concentrations of 2.2×10^{14}–4.9×10^{15} P/cm^3 and 3.5×10^{14}–6.5×10^{14} P/cm^3, respectively, using a Q-band ESR spectrometer (see Methods for details). These concentrations correspond to about 59 to 166 nm inter-donor distance assuming uniform distribution. The electric field is formed along the [100] crystal orientation by applying voltage between two 50-nm-thick aluminum plates sputtered on each face of the wafer. The direction of E_0 is coplanar to the external static magnetic field, and perpendicular to the oscillating microwave field (B_{mw}) as shown in Fig. 1.

For both samples, the electron spin echo signal decays in the T_1 measurement experiments are single exponential regardless of the magnitude of the electric field. On the other hand, when $E_0 = 0$, the T_2 decay curve is better described by $s(2\tau) = \exp[-(2\tau/T_{2a})^n - 2\tau/T_{2b}]$, where $s(2\tau)$ is the normalized electron spin echo signal with the interpulse delay τ[20]. However, we found that as the E_0 value reaches certain regime, the T_2 decay becomes a single exponential. In our measurements, the E_0 values from which the coherence decay curves are single exponential are 0.22 V/μm and 0.13 V/μm for sample A and B, respectively. Moreover, at these points, the T_1 relaxation times are significantly reduced. Figure 2 shows examples of electron spin signal decay from the T_1 [(a) and (b)] and T_2 [(c) and (d)] measurements for sample A with $E_0 = 0$ and 0.22 V/μm at $B_0 = 1.2$ T and 8 K. The inset in Fig. 2(c) shows that n estimated from fitting for several values of E_0 in the non-single exponential regime ranges between two to three, agreeing with previously reported values attributed to nuclear-induced spectral diffusion[3,20]. The large difference between the time scale (horizontal axis) of the figures on the left [(a) and (c)] and on the right [(b) and (d)] demonstrates the substantial increase of the relaxation rates when the electric field is turned on.

The relationship between E_0 and the relaxation times is plotted in Fig. 3. For A, T_1 is reduced by about three orders of magnitude at $E_0 \geq 0.22$ V/μm. The coherence decays fit well to single exponential in this regime, and T_2 appears to be limited by T_1. The solid line represents the magnitude of electric current between the metal plates, and shows the avalanche breakdown, a sudden transition to a low-resistance state, occurs at about 0.24 V/μm for this sample. Thus, E_0 could not be increased beyond this point. Interestingly, the relaxation times change dramatically even though the current is about two orders of magnitude smaller than that at the breakdown. The inset in Fig. 3(a) shows the relaxation times in A as a function of E_0 at 10 K to demonstrate that the effect persists in a different temperature. In this temperature and donor concentration, T_2 is limited by T_1 as the T_1 process dominates decoherence[6]. The relaxation times decrease rapidly as E_0 is increased beyond 0.15 V/μm, similar to the behaviour observed at 8 K. The electric field dependence of the relaxation times is qualitatively confirmed with the

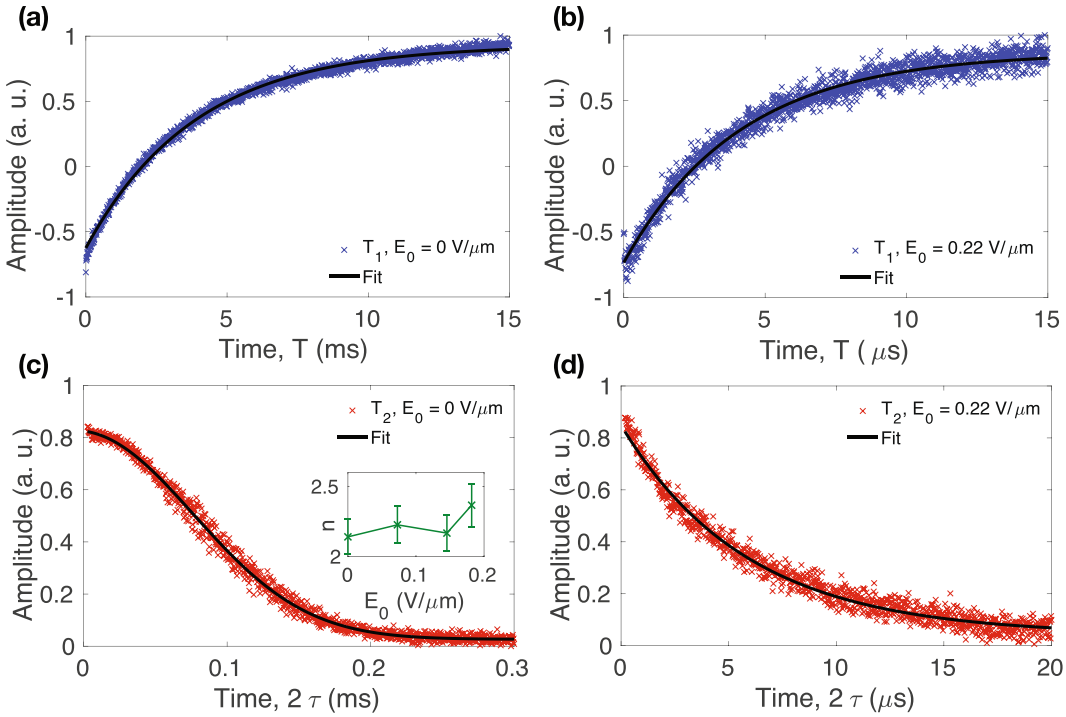

Figure 2. Examples of the electron spin echo decay to measure T_1 (**a**) without electric field, and (**b**) with $E_0 = 0.22$ V/μm, and to measure T_2 (**c**) without electric field, and (**d**) with $E_0 = 0.22$ V/μm for sample A at around 1.2 T and 8 K. The solid line in (**c**) is the fitting to $s(2\tau) = \exp[-(2\tau/T_{2a})^n - 2\tau/T_{2b}]$, and the inset shows the fitted values of n with the error bars representing the fitting error. The data in (**a**,**b** and **d**) are fitted using a single exponential decay curve.

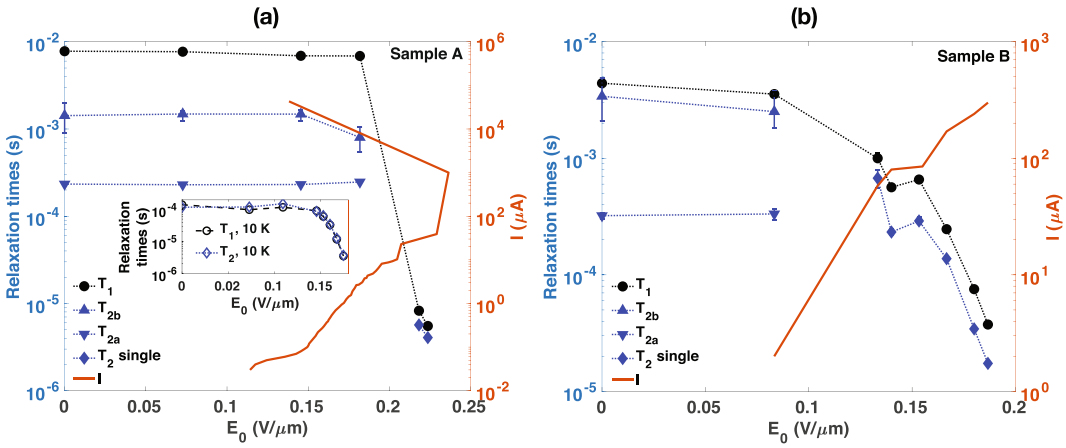

Figure 3. The electric field dependence of electron spin relaxation rates (left y-axis) for the Si:P sample (**a**) A and (**b**) B at near 1.2 T and 8 K. The inset in (**a**) shows the relaxation rates as a function of E_0 at 10 K. The circles represent the T_1 time, two triangle symbols are obtained from the non-exponential signal decay in the T_2 measurement, and the diamonds represent the T_2 time in the large electric field regime where the signal decay becomes single exponential. The solid lines (right y-axis) represent the electric current between two aluminum plates on the faces of the silicon wafer as a function of E_0. In (**a**), the avalanche breakdown occurs around 0.24 V/μm as indicated by the discontinuity in the current-electric field curve. The error bars represent fitting errors, and are smaller than the data symbol when not visible.

sample B as shown in Fig. 3(b). Both T_1 and T_2 do not exhibit noticeable changes until E_0 is increased up to about 0.08 V/μm. But from beyond this point, T_1 undergoes about two orders of magnitude reduction as E_0 is increased up to about 0.19 V/μm. Meanwhile, the T_2 decay converges to single exponential, and the spin coherence time appears to be limited by the T_1 process in this regime. The experimental data provide clear evidence that the longitudinal relaxation time of electron spins in Si:P is reduced substantially even when the applied electric field is smaller than the breakdown field. On the other hand, the impact of the electric field on T_2 independent from

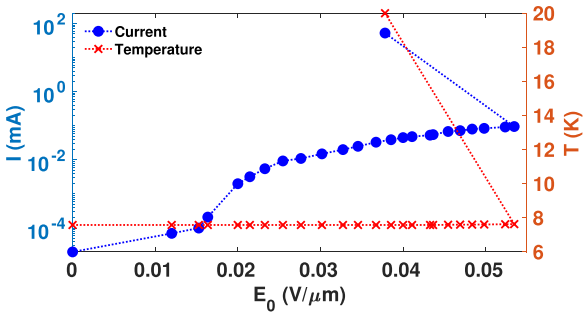

Figure 4. The electric current between two aluminum plates on the faces of the silicon sample A (left y-axis) and the sample temperature (right y-axis) as a function of the electric field strength, E_0. The avalanche breakdown is observed by the discontinuity in the current-electric field curve.

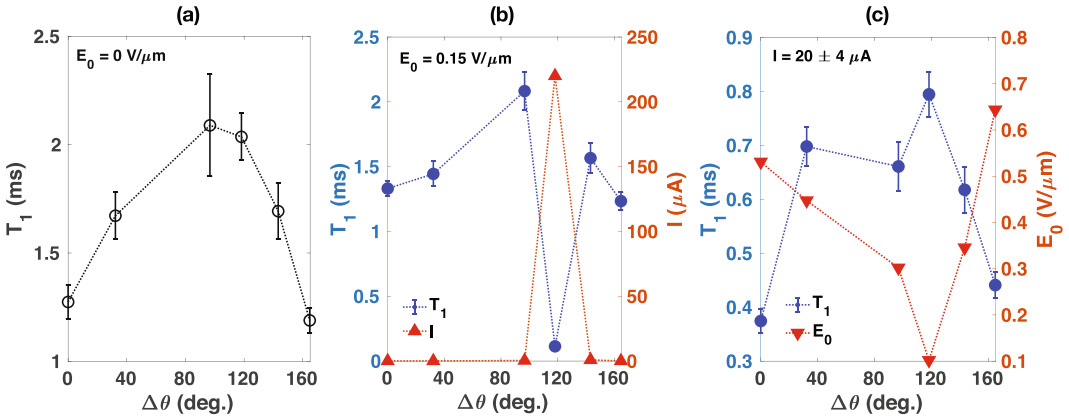

Figure 5. The T_1 relaxation times for the sample B (left y-axis) as a function of an angle between E_0 and B_0 when (**a**) $E_0 = 0$, (**b**) $E_0 = 0.15$ V/μm, and (**c**) $I = 20 \pm 4\,\mu$A. $\Delta\theta$ corresponds to the change of the angle between E_0 and B_0. For a fixed value of E_0, the electric current varies with the orientation, and vice versa. The anisotropy of the current and E_0 are presented in (**b**) and (**c**), respectively (right y-axis). The vertical error bars represent fitting errors. The uncertainty in $\Delta\theta$ is smaller than the width of the symbols.

the T_1 process is uncertain. The electric field effects on the spin relaxation times of the donor-bound electron in bulk silicon implies that the operating conditions of the Si:P quantum devices with higher donor densities can be limited due to accelerated decoherence. Hereinafter, we focus on the effect of the electric field on T_1.

In the temperature range in which the measurements are conducted, the strong temperature dependence of T_1 is known to exist due to spin-phonon relaxation process[21,22]. As a first step towards understanding the source of the electric field dependence of the relaxation times, we measured the sample temperature and the electric current in a Si:P wafer between two metal plates with respect to E_0 (see Methods). The measurement results depicted in Fig. 4 show that the sample temperature remains nearly constant until the breakdown field, at which the resistivity of the sample abruptly drops, is reached. Thus, the dramatic T_1 reduction in our measurements cannot be explained by the change in the sample temperature.

Next, we experimentally investigated the anisotropy of T_1 in the crystal orientation with respect to B_0 using B, the sample with more uniform donor distribution. In this study, the silicon crystal, and hence the direction of E_0, were rotated around the x-axis defined in Fig. 1 while the direction of B_0 was fixed. For each orientation, we conducted T_1 measurements with $E_0 = 0$, 0.15 V/μm, and at constant electric current of $20 \pm 4\,\mu A$ measured in the same direction as E_0. To maintain the constant electric current at each orientation, the strength of E_0 is adjusted by controlling the DC voltage. The results are shown in Fig. 5. Note that the independent variable in the figure ($\Delta\theta$) corresponds to the change of the angle between E_0 and B_0 from the reference angle determined by the initial sample placement in the magnetic field. The T_1 relaxation time is observed to be anisotropic in the crystal orientation, and hence the direction of E_0, with respect to B_0 in all experiments. For a fixed amount of E_0, we observed that the electric current in [100] direction also varied with respect to the orientation between E_0 and B_0. As shown in Fig. 5(b), when $E_0 = 0.15$ V/μm, the current is maximum near $\Delta\theta = 120°$. Interestingly, T_1 at this orientation is about an order of magnitudes smaller than that at other orientations. The anisotropic T_1 is also observed when the current is fixed at about 20 μA as illustrated in Fig. 5(c). In this case, however, the qualitative feature of the orientation dependence of T_1 resembles that of the orientation dependence observed when the electric field is turned off (Fig. 5(a)), except the relaxation times at each point are reduced by approximately a factor of three.

Discussion

The spin relaxation anisotropy without the electric field displayed in Fig. 5(a) is consistent with the previous results attributed to a modulation of the electronic g factor by acoustic phonons[23–25]. The previous studies show that the T_1 relaxation time is the longest when B_0 is aligned with [100] axis of the silicon crystal[25]. Thus, in our experimental data, the [100] axis lies within the range of $\Delta\theta = 96°$ to 118°.

Figure 5(b) shows that the electric current in the wafer between two metal plates is the largest when B_0 is aligned with [100] axis, along which E_0 is applied. The variation of the electric current with respect to the angle between E_0 and B_0 for a fixed electric field strength is consistent with the effect of magnetoresistance (MR), defined as $[R(B) - R(0)]/R(0)$, where $R(B)$ is the resistance in magnetic field B. The phosphorus density of sample B is just within the low doping regime where the MR for the perpendicular orientation ($B_0 \perp E_0$) is large[26]. For Si:P, the MR effect persists for the longitudinal orientation, i.e., $B_0 \| E_0$, since the Lorentz force can still deflect the carriers as the trajectories are distorted due to the random distribution of donors. Nevertheless, the longitudinal MR is known to be much smaller than the perpendicular MR[26,27]. Therefore, the large electric current at a specific orientation ($\Delta\theta \approx 118°$) can be interpreted as a consequence of the minimum MR since E_0 is parallel to B_0.

When $E_0 = 0.15$ V/μm, although the electric field is uniformly raised for all orientations, the T_1 time is significantly reduced only when the electric current is high. On the other hand, Fig. 5(c) shows that despite the large variation of E_0 with respect to the orientation, all relaxation times are about a factor of three smaller than the relaxation times at the same orientation without the electric field. These experimental results suggest that the acceleration of the longitudinal relaxation rate at strong electric field is related to the rise of the electric current in the Si:P crystal rather than the strength of the electric field.

The quality of the electron spin qubits in Si:P can be degraded considerably when large electric field is needed, due to the increased decoherence rate. In order to enhance the utility and the flexibility of the donor-based spin qubits, it is desirable to extend the high-fidelity qubit operating range to strong electric fields. Moreover, there exists an architectural proposal that demands the application of strong electric fields so that the electron spins are manipulated near the ionization point[16]. Therefore, finding strategies to circumvent the escalation of the spin relaxation rates is critical. From above experimental studies, we found that the electric current, rather than the electric field, is responsible for the rapid change in T_1. Then we experimentally verified that MR yields the electric current anisotropy in the orientation of E_0 with respect to the external magnetic field. Therefore, if the angle between E_0 and B_0 is chosen properly, the electric current for a given E_0 strength, and hence the reduction in the T_1 time can be minimized. In particular, the electric field should not be aligned with the magnetic field. For instance, Fig. 5(b,c) illustrate that when E_0 is nearly parallel to B_0 ($\Delta\theta \approx 120°$), T_1 is about 0.1 ms for $E_0 = 0.15$ V/μm, while when E_0 is nearly perpendicular to B_0 ($\Delta\theta \approx 40°$), T_1 is about 0.7 ms for $E_0 = 0.45$ V/μm. Thus, in this example data, the T_1 time at one orientation can be about seven times longer than that at another orientation, although about three times larger E_0 is used. Recall that in the absence of E_0, the T_1 time is the longest when B_0 is applied along the [100] direction. Thus, we speculate that further T_1 optimization is possible by using a silicon wafer grown in a direction such that the direction of B_0 can be parallel to [100], but perpendicular to E_0.

In summary, the T_1 relaxation rate of the phosphorus donor electron spins in bulk silicon with low dopant concentration can be increased significantly under large electric fields due to electric current in the sample. The coherence time is also shortened as it is upper-bounded by T_1. On the other hand, the amount of electric current is anisotropic in the E_0 orientation with respect to the external magnetic field due to the MR effect. Thus, the reduction in the relaxation rates for a fixed electric field strength can be minimized by choosing the appropriate orientation. Although the decoherence rate must be minimized during quantum gate operations, the fast T_1 relaxation can be exploited in a special instance. Namely, when the qubit initialization method relies on thermal equilibration, the fast relaxation rate is favoured for resetting the qubits. Furthermore, the ability to engineer the T_1 relaxation rate can be useful for dynamic nuclear polarization since the increased T_1 rate allows for the faster polarization of nuclear spins at the cost of the higher microwave pulse power for saturating the electron spin transitions[28]. Future work could extend the range of the experimental conditions, such as the magnetic field strength, the temperature, and the donor density. Our results also motivate further studies on the nuclear spin relaxation rates, as well as the case of the single donor spins in large electric fields.

Methods

Sample preparation. Two commercially purchased phosphorus doped (100)-silicon wafers with natural abundance (4.7% of ^{29}Si) are used throughout the experiments. The first wafer (A) is quoted with the room temperature resistivity of 1–20 Ω·cm (about 2.2×10^{14}–4.9×10^{15} P/cm^3), and the thickness of 275 μm. The second wafer (B) has the room temperature resistivity of 7–13 Ω·cm (about 3.5×10^{14}–6.5×10^{14} P/cm^3), and is 300 μm thick. The wafers are cut to a size of approximately 1×15 mm to fit in a standard Q-band ESR tube.

Electron spin resonance measurements. All ESR experiments were carried out at Korea Basic Science Institute (KBSI) in Seoul, Korea. 34 GHz Q-band pulsed ESR data were obtained on a Bruker Elexsys E580 spectrometer using an EN5107D2 resonator. Cryogenic temperatures were achieved with an Oxford CF-935 cryostat and an Oxford ITC temperature controller.

Relaxation times measurements. T_1 is measured via inversion recovery experiment, and T_2 is measured via Hahn echo decay experiment. The pulse sequence for the inversion recovery experiment can be expressed as $\pi - T - \pi/2 - \tau - \pi - \tau -$echo detection. The delay, T, after the first π pulse was varied while τ was fixed, and the amplitude of the primary echo signal formed by the second and third pulses was measured. The pulse sequence for the Hahn echo decay experiment is $\pi/2 - \tau - \pi - \tau -$echo detection, and the amplitude of the echo signal was measured as a function of the delay, τ. The $\pi/2$ and π pulse lengths were 16 and 32 ns, respectively, in both experiments.

Current-voltage measurements. The current-voltage relations are measured using two multimeters (Fluke 287 True-RMS), each connected in parallel and in series with the silicon wafer for measuring voltage and current, respectively.

Sample temperature measurements. The sample temperature dependence on the electric field strength was measured with an Si:P piece cut from A to an approximate size of 1 cm^2. A calibrated temperature sensor (Lakeshore DT-470-CU-13) was attached on top of the aluminum on one face of the wafer, and the other face of the wafer was in contact with the copper heat-sink of a low temperature probe. Then the probe was cooled using a helium-flow cryostat. The current was measured using a multimeter while external DC voltage was applied.

Data Availability

The datasets generated during and/or analysed during the current study are available from the corresponding author on reasonable request.

References

1. Kane, B. E. A silicon-based nuclear spin quantum computer. *Nat.* **393**, 133 (1998).
2. Tyryshkin, A. M., Lyon, S. A., Astashkin, A. V. & Raitsimring, A. M. Electron spin relaxation times of phosphorus donors in silicon. *Phys. Rev. B* **68**, 193207, https://doi.org/10.1103/PhysRevB.68.193207 (2003).
3. Tyryshkin, A. M. *et al.* Coherence of spin qubits in silicon. *J. Physics: Condens. Matter* **18**, S783 (2006).
4. Muhonen, J. T. *et al.* Storing quantum information for 30 seconds in a nanoelectronic device. *Nat. Nanotechnol.* **9**, 986 (2014).
5. Itoh, K. M. & Watanabe, H. Isotope engineering of silicon and diamond for quantum computing and sensing applications. *MRS Commun.* **4**, 143–157, https://doi.org/10.1557/mrc.2014.32 (2014).
6. Tyryshkin, A. M. *et al.* Electron spin coherence exceeding seconds in high-purity silicon. *Nat. Mater.* **11**, 143 EP (2011).
7. Morello, A. *et al.* Single-shot readout of an electron spin in silicon. *Nat.* **467**, 687 (2010).
8. Pla, J. J. *et al.* A single-atom electron spin qubit in silicon. *Nat.* **489**, 541 (2012).
9. Pla, J. J. *et al.* High-fidelity readout and control of a nuclear spin qubit in silicon. *Nat.* **496**, 334 (2013).
10. Muhonen, J. T. *et al.* Quantifying the quantum gate fidelity of single-atom spin qubits in silicon by randomized benchmarking. *J. Physics: Condens. Matter* **27**, 154205 (2015).
11. Wolfowicz, G. *et al.* Conditional control of donor nuclear spins in silicon using stark shifts. *Phys. Rev. Lett.* **113**, 157601, https://doi.org/10.1103/PhysRevLett.113.157601 (2014).
12. Laucht, A. *et al.* Electrically controlling single-spin qubits in a continuous microwave field. *Sci. Adv.* **1**, https://doi.org/10.1126/sciadv.1500022. http://advances.sciencemag.org/content/1/3/e1500022.full.pdf (2015).
13. Hill, C. D. *et al.* A surface code quantum computer in silicon. *Sci. Adv.* **1**, https://doi.org/10.1126/sciadv.1500707. http://advances.sciencemag.org/content/1/9/e1500707.full.pdf (2015).
14. O'Gorman, J., Nickerson, N. H., Ross, P., Morton, J. J. & Benjamin, S. C. A silicon-based surface code quantum computer. *npj Quantum Inf.* **2**, 15019 (2016).
15. Pica, G., Lovett, B. W., Bhatt, R. N., Schenkel, T. & Lyon, S. A. Surface code architecture for donors and dots in silicon with imprecise and nonuniform qubit couplings. *Phys. Rev. B* **93**, 035306, https://doi.org/10.1103/PhysRevB.93.035306 (2016).
16. Tosi, G. *et al.* Silicon quantum processor with robust long-distance qubit couplings. *Nat. Commun.* **8**, 450, https://doi.org/10.1038/s41467-017-00378-x (2017).
17. Boross, P., Széchenyi, G. & Pályi, A. Valley-enhanced fast relaxation of gate-controlled donor qubits in silicon. *Nanotechnol.* **27**, 314002 (2016).
18. Delmo, M. P., Kasai, S., Kobayashi, K. & Ono, T. Current-controlled magnetoresistance in silicon in non-ohmic transport regimes. *Appl. Phys. Lett.* **95**, 132106, https://doi.org/10.1063/1.3238361 (2009).
19. Delmo, M. P., Yamamoto, S., Kasai, S., Ono, T. & Kobayashi, K. Large positive magnetoresistive effect in silicon induced by the space-charge effect. *Nat.* **457**, 1112 (2009).
20. Abe, E. *et al.* Electron spin coherence of phosphorus donors in silicon: Effect of environmental nuclei. *Phys. Rev. B* **82**, 121201, https://doi.org/10.1103/PhysRevB.82.121201 (2010).
21. Feher, G. & Gere, E. A. Electron spin resonance experiments on donors in silicon. ii. electron spin relaxation effects. *Phys. Rev.* **114**, 1245–1256, https://doi.org/10.1103/PhysRev.114.1245 (1959).
22. Castner, T. G. Orbach spin-lattice relaxation of shallow donors in silicon. *Phys. Rev.* **155**, 816–825, https://doi.org/10.1103/PhysRev.155.816 (1967).
23. Hasegawa, H. Spin-lattice relaxation of shallow donor states in ge and si through a direct phonon process. *Phys. Rev.* **118**, 1523–1534, https://doi.org/10.1103/PhysRev.118.1523 (1960).
24. Roth, L. M. g factor and donor spin-lattice relaxation for electrons in germanium and silicon. *Phys. Rev.* **118**, 1534–1540, https://doi.org/10.1103/PhysRev.118.1534 (1960).
25. Wilson, D. K. & Feher, G. Electron spin resonance experiments on donors in silicon. iii. investigation of excited states by the application of uniaxial stress and their importance in relaxation processes. *Phys. Rev.* **124**, 1068–1083, https://doi.org/10.1103/PhysRev.124.1068 (1961).
26. Porter, N. A. & Marrows, C. H. Dependence of magnetoresistance on dopant density in phosphorous doped silicon. *J. Appl. Phys.* **109**, 07C703, https://doi.org/10.1063/1.3536663 (2011).
27. Wang, T. *et al.* Angular dependence of the magnetoresistance effect in a silicon based p–n junction device. *Nanoscale* **6**, 3978–3983, https://doi.org/10.1039/C3NR04077A (2014).
28. Järvinen, J. *et al.* Efficient dynamic nuclear polarization of phosphorus in silicon in strong magnetic fields and at low temperatures. *Phys. Rev. B* **90**, 214401, https://doi.org/10.1103/PhysRevB.90.214401 (2014).

Acknowledgements

We thank Sungmin Kwon and Sumin Lim for helpful discussions, and Donghyuk Jeong and Yujeong Kim for operating the ESR spectrometer at KBSI. This research was supported by the National Research Foundation of Korea (Grants No. 2015K1A31A14021146, 2015R1A2A2A01006251, and 2016R1A5A1008184).

Author Contributions

S.L. conceived the project. D.K.P., S.P. and H.J. conducted the experiments. D.K.P., S.P. and S.L. analysed and discussed the results. All authors reviewed the manuscript.

Additional Information

Competing Interests: The authors declare no competing interests.